Mechanisms and kinetics of the inhibition layer breakdown in the case of Ti IF steel grades galvanized in GA baths

D. Zapico Álvarez, Florence Bertrand, J.-M. Mataigne, M.-L. Giorgi

Mechanisms and kinetics of the inhibition layer breakdown in the case of Ti IF steel grades galvanized in GA baths

D. Zapico Álvarez[1], F. Bertrand[1], J.-M. Mataigne[1], M.-L. Giorgi[2]

[1] ArcelorMittal Global R&D, Maizières Automotive Products,
Voie Romaine BP 30320, 57283 Maizières-Lès-Metz, France
Phone: +33 (0)3 87 70 76 77, Email: david.zapico@arcelormittal.com
Phone: +33 (0)3 87 70 48 96, Email: florence.bertrand@arcelormittal.com
Phone: +33 (0)3 44 55 73 69, Email: jean-michel.mataigne@arcelormittal.com

[2] École Centrale Paris, Laboratoire de Génie des Procédés et Matériaux,
Grande Voie des Vignes, 92295 Châtenay-Malabry cedex, France
Phone: +33 (0)1 41 13 11 72, Email: marie-laurence.giorgi@ecp.fr

ABSTRACT

A reaction mechanism is proposed accounting for the inhibition layer breakdown in the case of Ti IF steels. This mechanism can be summarized in two steps: 1) the transformation of the bi-layered inhibition layer into a mono-layered one, made of the δ ($FeZn_7$) phase only, as a result of the Zn enrichment at the steel/inhibition layer interface, and 2) the local nucleation of the Γ (Fe_3Zn_{10}) phase at the steel grain boundaries, breaking the δ layer off, when the Zn concentration at these locations becomes high enough (outburst formation). The kinetics of this reaction strongly depends on the Ti IF steel chemistry. The effect of the steel chemical composition on the inhibition layer breakdown kinetics would be ruled by the rate of Zn diffusion at the steel grain boundaries and the ability of the steel to accumulate the Zn atoms within a critical volume for the nucleation of Γ phase at these locations.

Keywords: Al-Fe-Zn ternary system, interfacial reactions, galvannealing, inhibition layer, inhibition breakdown

INTRODUCTION

The development of a conventional GalvAnnealed (GA) coating on a Ti-stabilized Interstitial Free (Ti IF) steel grade passes through different and complex reactions: the inhibition layer formation, the inhibition layer breakdown, the liquid Zn consumption and the enrichment in Fe of the coating by solid state diffusion. A fine knowledge of the kinetics of each of these reactions may considerably help process and production engineers to define the thermal cycle allowing reaching the customer targets in terms of iron content and Fe-Zn phase distribution within the coating.

A very thin layer of Al-rich intermetallic compounds nucleates very rapidly (around 0.1 - 0.2 s [1)]) on the steel surface during galvanizing in Al-containing Fe-saturated Zn baths. This layer is commonly known as *inhibition layer*, as it inhibits, at least temporarily, the alloying reactions between Fe and Zn. It has been demonstrated in a previous study [2)] that the inhibition layer which forms in typical baths for galvannealing production (Fe-saturated Zn baths with Al content ranging from 0.10 to 0.135 wt.% at 460 °C) is actually composed of a very thin layer of $Fe_2Al_5Zn_x$ (becoming discontinuous for low Al contents) and a thicker layer of Al-saturated δ ($FeZn_7$) on its top. This microstructure allows thermodynamic equilibrium to be reached along all interfaces and the system does therefore not require any other interfacial reaction.

However, increased temperature in the induction furnace, located at the exit of the galvanizing bath, activates Fe and Zn inter-diffusion through the inhibition layer and, after a while, this layer is destabilized. This reaction, called the *inhibition layer breakdown*, is a key step in the galvannealing process as it leads to the sudden development of Fe-Zn phases by consuming liquid Zn. It is therefore crucial to understand the mechanisms and kinetics of this reaction.

Different mechanisms have been proposed in the literature to explain the inhibition layer breakdown. Even if a very small group of researchers [3,4)] reported that the Fe-Zn reactions are activated by the dissolution of the inhibition layer in liquid Zn, it is generally admitted that an outburst reaction is the responsible for the inhibition layer breakdown in the case of Ti IF steels [5-18)]. Two mechanisms can be found to explain the outburst formation. A few researchers [5-7)] submitted that the diffusion of Fe towards liquid Zn causes the growth of the inhibition layer and, as a result, an Al depletion at the solid / liquid interface, leading to the outburst formation. A much more important group of researchers [8-18)] reported that the triggering phenomenon in the mechanism of outburst formation is the diffusion of Zn towards the steel substrate. Nishimoto *et al.* [5)] were the first researchers to reveal that the outbursts are formed at the steel grain boundaries for long

immersion times in GA baths. Hisamatsu [8] confirmed afterwards that the steel grain boundaries are preferential locations for outburst formation. Later, other authors [9,10] provided new experimental evidence of the formation of outbursts at the emergence of the steel grain boundaries.

The kinetics of the inhibition layer breakdown is strongly influenced by the galvanizing conditions and the base steel features. It is well known that the higher the Zn bath Al content, the slower the inhibition layer breakdown kinetics [9]. As for the steel substrate, it is generally admitted that the finer the grain size, the faster the inhibition layer breakdown occurs [8,11,12,19]. The steel chemical composition also plays an important role on the kinetics of the inhibition layer breakdown. Elements such as C, N, S and P may segregate to the steel grain boundaries during recrystallization annealing, hindering the diffusion of Zn at these locations and therefore delaying the inhibition layer breakdown [5,8,9,13-16,19]. On the contrary, Ti can precipitate with the previous elements, limiting their segregation in solid solution at the steel grain boundaries and, therefore, promoting their cleanliness and a faster inhibition layer breakdown [5,8,13,15,19,20]. In this work, the reactivity of Ti IF steels will be assessed by calculating the excess solute Ti in mole fraction, $x_{Ti_{excess}}$, assuming full precipitation of TiC, TiN and TiS and partial precipitation of FeTiP, which is somewhat different to what was proposed by Toki *et al.* [19].

$$x_{Ti_{excess}} = \left(w_{Ti_{total}} - \frac{48}{12} w_C - \frac{48}{14} w_N - \frac{48}{32} w_S \right) \times \frac{31}{48 w_P} \qquad (1)$$

where $w_{Ti_{total}}$, w_C, w_N, w_S and w_P are the weight fractions of Ti, C, N, S and P present in the steel.

The main objective of this work is to study the mechanisms and the kinetics of the inhibition layer breakdown in the case of Ti IF steels with different excess solute Ti. The work is divided into the following stages: 1) the inhibition layer formed on steel samples galvanized in a Zn bath with 0.127 wt.% Al was observed; the evolution of this inhibition layer was then observed when the galvannealing temperature was increased; 2) the time needed for the inhibition layer breakdown was measured as a function of galvannealing temperature and excess solute Ti of the steel; 3) key mechanisms accounting for the inhibition layer breakdown were proposed together with a simple model to predict the time needed for the inhibition layer breakdown.

EXPERIMENTAL PROCEDURE

Four different commercial Ti IF full hard steels, A, B, C and D, have been selected for this study. The thicknesses of these steels are very similar and equal to 0.75, 0.70, 0.74 and 0.74 mm respectively. Their average chemical composition is shown in table 1 together with their excess solute Ti (equation 1). The analysis was performed by means of Combustion and Infrared Detection for nitrogen (HORIBA EMGA-620W) and Spark-OES (SPECTROLAB M10) for the other elements in ArcelorMittal laboratories.

Table 1 Average chemical composition (x 10^{-3} wt.%) of the Ti IF steels studied.

Steel	C	Mn	P	S	N	Si	Cu	Ni	Cr	Sn	As	Nb	Mo	B	Ti	Al	$x_{Ti_{excess}}$ *
A	3.0	100.2	12.4	14.1	3.4	9.3	25.5	17.4	21.8	5.7	2.7	0.1	2.6	0.5	57.4	44.6	0.7
B	2.1	89.9	13.6	15.2	3.9	4.0	24.8	13.9	22.3	3.0	1.8	-	2.2	-	83.6	29.1	1.8
C	2.0	110.0	9.1	9.0	2.1	4.0	17.0	14.3	18.2	5.7	-	0.1	1.8	0.0	67.3	49.1	2.7
D	2.2	99.9	6.9	12.5	3.4	4.6	36.6	20.3	27.9	3.9	2.0	0.1	1.9	-	84.1	55.8	4.2

* expressed in mole fraction

The commercial steel sheets were cut into samples with dimensions of 210 x 99 mm^2. These samples were cleaned with ethanol to remove residual oil from former manipulations. Samples were then annealed at 800 °C under controlled atmosphere of N_2 and 5 vol.% H_2 with -60 °C dew point and galvanized in a Rhesca Hot Dip Process simulator. The galvanizing conditions are summarized in table 2.

Samples galvanized in the Rhesca simulator were then cut into samples with dimensions of 120 x 30 mm^2 and submitted to isothermal heat treatments in a Gleeble 3500 device, able to provide very high heating and cooling rates (around 200 °C/s) as well as very steady and accurate holding temperatures and times. The isothermal treatments were performed on each steel at holding temperatures of 430, 445 and 460 °C and several times in order to determine accurately the time needed to achieve the inhibition layer breakdown at each of these temperatures. In the case of steel C, supplementary

holding temperatures of 425, 438 and 452 °C have been tested in order to confirm the tendencies observed. The thermal homogeneity area in the Gleeble 3500 samples was defined on the basis of a thermal homogeneity criterion of ± 5 °C and corresponded to a squared area of 10 x 10 mm^2 in the centre of the sample, where the thermocouple was placed. It is obviously in this area of the sample that the characterizations have been done.

Table 2 Galvanizing conditions for the Ti IF steels studied.

w_{Al} (wt.%) [a]	T_{bath} (°C) [b]	t_{im} (s) [c]
0.127 ± 0.003	460 ± 2	0.7

[a] bath aluminium content; [b] bath temperature; [c] immersion time.

Some cross-section specimens were prepared by Ar ion beam Cross Section Polishing (CSP, JEOL SM-09010) and characterized in a Scanning Electron Microscope (SEM, JEOL JSM-7001F) in order to check the structure of the inhibition layer on the galvanized samples before heat treatment in the Gleeble 3500 pilot.

The state of the inhibition layer of the samples annealed in the Gleeble 3500 pilot was characterized through SEM (LEO DSM 982) observations of the sample surface after selective electrochemical dissolution. The electrochemical cell used for these dissolutions was composed of three electrodes: a standard calomel electrode (SCE) used as reference electrode, a Pt counter electrode used as cathode and the sample to be dissolved in the form of a 32 mm diameter disc (working electrode) used as anode. The electrolyte used is an aqueous pH 4 solution composed of 200 g/L NaCl (Fisher Chemical), 40 g/L $ZnSO_4 \bullet 7H_2O$, 27 g/L CH_3COONa and 11 mL/L CH_3COOH (VWR BDH Prolabo). The electrochemical potential to be imposed in order to achieve the selective removal of Zn and Al-free Fe-Zn phases is -800 mV. In these conditions, the whole inhibition layer (Al-saturated δ and $Fe_2Al_5Zn_x$) is kept at the sample surface because of its high Al content.

The inhibition layer breakdown is said to have occurred when holes in the inhibition layer, created by outbursts formation at the steel grain boundaries, are observed. The determination of the inhibition layer breakdown by surface SEM observations is illustrated in figure 1, where an example corresponding to steel B annealed in the Gleeble 3500 device at 430 °C for 30 (left; intact inhibition layer) and 35 s (right; broken inhibition layer) is shown. The diffusion of Zn through the inhibition layer, leading to its breakdown, mainly takes place during annealing in the Gleeble device but may begin during galvanizing and cooling down in the Rhesca simulator. This part of the diffusion process is minimized by using a short immersion time (0.7 s) followed by a forced cooling (6 °C/s). As explained later, the measured experimental time needed for the inhibition layer breakdown is corrected to take into account the diffusion of Zn in the Rhesca simulator.

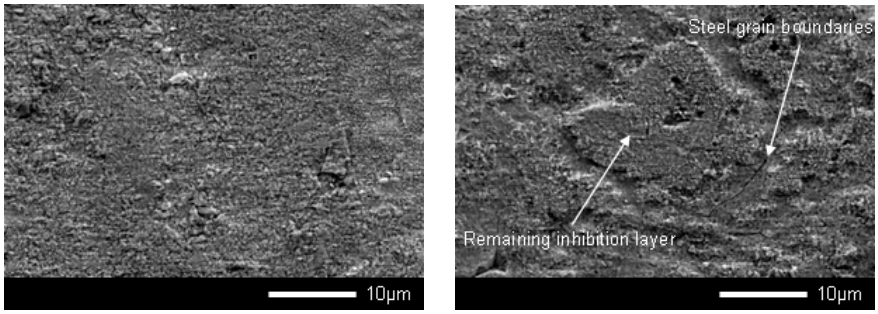

Figure 1 Surface SEM micrographs of steel B annealed in the Gleeble 3500 pilot at 430 °C for 30 (left; intact inhibition layer) and 35 s (right; broken inhibition layer).

In order to understand the mechanisms accounting for the inhibition layer breakdown, mechanically polished cross-section specimens were also prepared from some well-chosen samples that had only known the inhibition layer breakdown after heat treatment in the Gleeble 3500 device in the thermal homogeneity area but not elsewhere (lower temperature compared to the centre of the sample). The cross-section specimens were prepared from samples taken at different positions along the longitudinal axis of the original Gleeble 3500 samples and characterized by Energy Dispersive Spectroscopy (EDS, Bruker AXS XFlash 4010 SDD) in a SEM (JEOL JSM-7001F).

EXPERIMENTAL RESULTS

The structure of the inhibition layer on the samples galvanized in the Rhesca simulator has been found to be totally consistent with the one observed in a previous study [2)] on a steel galvanized with the same bath temperature and aluminum content (table 2) in industrial line: the inhibition layer is in both cases composed of a very thin continuous

$Fe_2Al_5Zn_x$ layer and a thicker δ layer on its top. The presence of isolated ζ rod crystal has also been observed (figure 2).

Cross-section samples were characterized at different locations along the longitudinal axis of a Gleeble sample after galvanizing in the Rhesca simulator and annealing at 430 °C for 60 s in the Gleeble 3500 device (figure 3). A gradient of temperature existed from the left-hand side (lowest temperature) to the right-hand side (highest temperature) micrographs. At the lowest temperature (figure 3a), the Zn coating remained solid and no diffusion phenomena could be observed: the inhibition layer is still composed of a very thin continuous layer of $Fe_2Al_5Zn_x$ and a thicker layer of δ on its top. At intermediate temperature (figure 3b), the Zn coating was liquid and the diffusion of Fe from the steel to the coating took place with two consequences: 1) the growth of the δ phase can be observed and 2) the Fe supersaturation present in the coating leads to the formation of a large amount of evanescent ζ crystals on top of the δ phase during the fast cooling. At the same time, diffusion of Zn from the coating to the steel led to the complete disappearance of the thin layer of $Fe_2Al_5Zn_x$, replaced by δ. As the inhibition layer is now composed of the δ phase only, the associated EDS signal for Al is thicker but less intense than in figure 3a. At the highest temperature, here equal to 430 °C (figure 3c), an outburst can clearly be observed and almost no Al is detected by EDS mapping analysis.

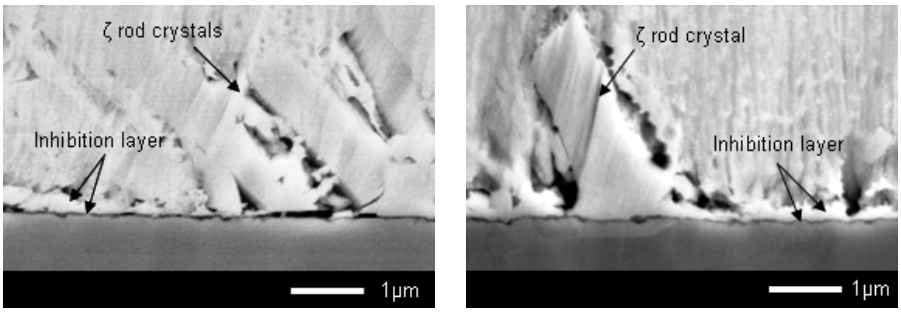

Figure 2 Cross-section SEM micrographs of the inhibition layers obtained on a sample galvanized in the Rhesca simulator (left) and on a sample from a previous study [2] galvanized with the same conditions in industrial line (right).

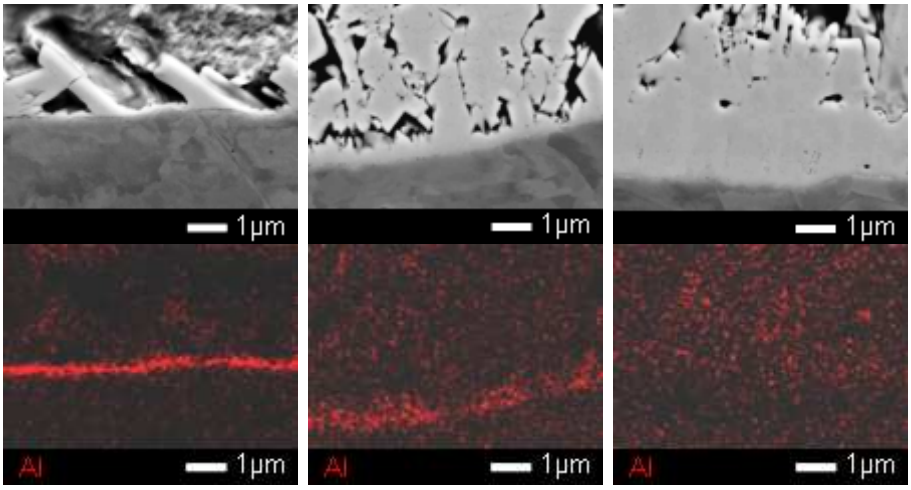

(a) (b) (c)

Figure 3 Cross-section SEM micrographs and EDS mappings for Al for samples taken at different locations along the longitudinal axis of a Gleeble sample: (a) lowest temperature, (b) intermediate temperature, (c) highest temperature equal to 430 °C (steel A galvanized in the Rhesca simulator and annealed in the Gleeble 3500 device at 430 °C for 60 s).

The experimental holding time performed in the Gleeble 3500 pilot necessary for the inhibition rupture $t_{hold,exp}$ is plotted against the experimental holding temperature $T_{hold,exp}$ in figure 4 for each of the Ti IF steels studied. The uncertainty in each point represents the difference between the highest holding time for which the inhibition rupture has not occurred yet and the lowest time for which the inhibition rupture has been observed. The time for inhibition breakdown has been chosen as the point in the middle of the interval defined by these two times. It is obvious that the smaller this interval, the more accurate the determination of the time for inhibition breakdown, but a compromise between accuracy and number of trials had to be found. At least in the range of the temperatures tested, the steel reactivity classification is as expected according to the values of $x_{Ti_{excess}}$ (table 1): steel D is more reactive (the inhibition layer breakdown is achieved faster) than steel C and this latter is more reactive than steel B, steel A being the less reactive one.

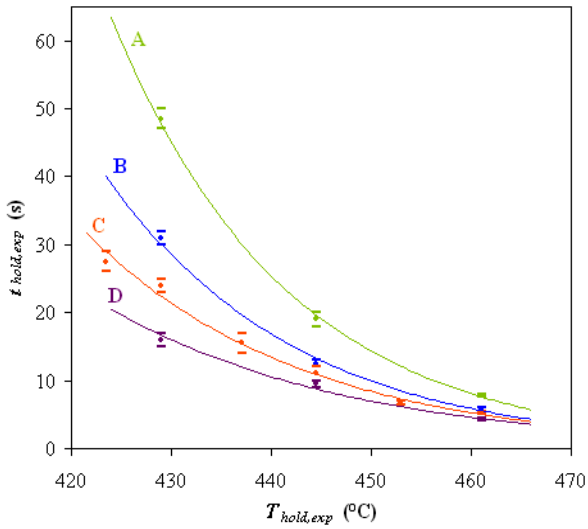

Figure 4 Experimental holding time needed for the inhibition layer breakdown against the experimental holding temperature performed in the Gleeble 3500 pilot.

DISCUSSION

The mechanisms accounting for the inhibition layer breakdown can be explained by means of the concept of diffusion paths in the Al-Fe-Zn ternary phase diagram at the holding temperature (figure 5).

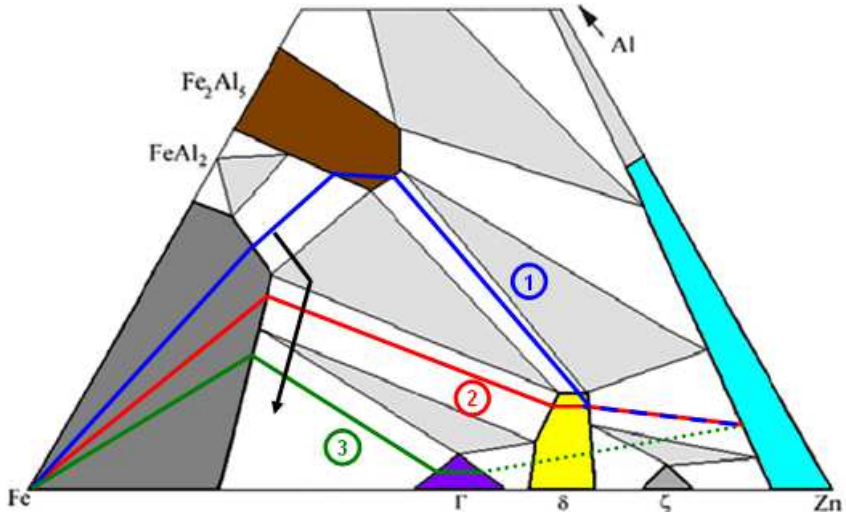

Figure 5 Schematic representation of diffusion paths in the Al-Fe-Zn ternary phase diagram at the holding temperature describing the mechanisms accounting for the inhibition layer breakdown.

The initial state of the inhibition layer can be described by diffusion path 1, which illustrates a microstructure with all its interfaces (steel / $Fe_2Al_5Zn_x$, $Fe_2Al_5Zn_x$ / δ, δ / liquid Zn) at thermodynamic equilibrium (figures 2 and 3a) [2].

During the galvannealing heat treatment, the inhibition layer grows by Fe diffusion towards the liquid Zn. At the same time, Zn diffuses towards the steel matrix. The steel / $Fe_2Al_5Zn_x$ interface gets progressively enriched in Zn or, what is the same, impoverished in Al (black arrow in figure 5). The $Fe_2Al_5Zn_x$ phase disappears and thermodynamic equilibrium between steel and δ is reached along the steel / inhibition layer interface (figure 3b). This microstructure is represented by the diffusion path 2 in figure 5.

During all this time, the steel grain boundaries are short-circuit diffusion paths for Zn and become preferentially enriched in this element. When the Zn concentration at these locations is high enough, the steel / δ interface is locally destabilized: the diffusion path crosses the ternary domain involving Fe, δ and Γ. The Γ phase therefore nucleates at the steel grain boundaries. Its volume expansion breaks the δ layer off locally and the Γ phase gets in direct contact with liquid Zn. This

microstructure is represented by path 3, where the dotted line indicates that no equilibrium is possible between the Γ phase and liquid Zn. This non-equilibrium situation would lead to the dissolution of the Γ phase surface and the nucleation of new Fe-Zn phases on its top. This microstructure, commonly known as outburst, is not discussed here as the present analysis focuses only on the phenomena taking place until the inhibition breakdown occurs.

A model describing the inhibition layer breakdown kinetics through outburst formation is presented below. The constants of this model were determined from the experimental results shown in figure 4. Due to the complexity of the reaction mechanisms proposed above for the inhibition layer breakdown, the following simplifications were made in order to facilitate modeling work:

- The Fe diffusion is neglected so that the thickness of the inhibition layer can be considered constant.
- The rate of Zn diffusion from the middle of the steel grains towards the grain boundaries is assumed to be infinite, so that the Zn concentration along the steel / inhibition layer interface can be assumed constant.
- The diffusion of Zn through the $Fe_2Al_5Zn_x$ and δ layers is described by a global diffusion coefficient taking into account the Zn diffusion in the entire inhibition layer.

Based on these assumptions, a simplified diffusion model can be proposed from Fick's law in steady state. The Zn diffusion flux through the inhibition layer $\phi_{Zn}^{i.l.}$ (mol m^{-2} s^{-1}) can be expressed as follows:

$$\phi_{Zn}^{i.l.} = -D_{Zn}^{i.l.} \nabla c_{Zn}^{i.l.} = D_{Zn}^{i.l.} \left|\nabla c_{Zn}^{i.l.}\right| = D_0 \exp\left(\frac{-E_a}{RT}\right)\left|\nabla c_{Zn}^{i.l.}\right| \quad (2)$$

where $D_{Zn}^{i.l.}$ (m^2 s^{-1}) is the diffusion coefficient of Zn in the inhibition layer, whose variation with temperature T has been expressed through an Arrhenius equation, D_0 (m^2 s^{-1}) being the pre-exponential factor, E_a (J mol^{-1}) the activation energy for diffusion and R (J mol^{-1} K^{-1}) the universal gas constant. As the Zn concentrations along all interfaces of the inhibition layer and its thickness are assumed to be constant, the Zn concentration gradient in the inhibition layer $\nabla c_{Zn}^{i.l.}$ is also constant.

The critical time at which the inhibition layer breakdown is achieved t_c (s) is such that a critical quantity of Zn Q_c (mol m^{-2}) diffuses through the inhibition layer. For a given steel, this critical quantity is expected to be constant, independent of time:

$$Q_c = \int_{t_{growth}}^{t_c} \phi_{Zn}^{i.l.}\, dt = D_0 \left|\nabla c_{Zn}^{i.l.}\right| \int_{t_{growth}}^{t_c} \exp\left(\frac{-E_a}{RT}\right) dt \quad (3)$$

where t_{growth} (s) is the time necessary for the growth of a covering inhibition layer (around 0.1 - 0.2 s after the steel strip enters the galvanizing bath [1)]). Both parameters E_a and $Q_c \Big/ \left(D_0 \left|\nabla c_{Zn}^{i.l.}\right|\right)$ were obtained experimentally.

For isothermal annealing treatments, the activation energy E_a can be directly extracted from the slope of straight lines expected to be obtained when representing the results of figure 4 in the form of experimental holding time in logarithmic scale against the reciprocal of the holding temperature:

$$\ln t_{hold,\exp} = \ln\left(\frac{Q_{hold,\exp}}{D_0 \left|\nabla c_{Zn}^{i.l.}\right|}\right) + \frac{E_a}{RT_{hold,\exp}} \quad (4)$$

where $Q_{hold,exp}$ is the part of the critical quantity of Zn that diffuses through the inhibition layer to the steel grain boundaries during the isothermal treatment.

The parameter $Q_c \Big/ \left(D_0 \left|\nabla c_{Zn}^{i.l.}\right|\right)$ cannot be determined from the y-intercept values of these straight lines (equation 4) because Zn has already diffused during galvanizing in the Rhesca pilot simulator. The real time for the inhibition layer breakdown t_c is therefore underestimated when represented by $t_{hold,exp}$. As a result, this latter needs to be corrected by

taking into account the diffusion of Zn during the Rhesca thermal cycle, which can be calculated by integrating the right hand side expression of equation 3 along the Rhesca thermal cycle (immersion in the galvanizing bath and subsequent cooling) once E_a has been obtained.

Finally, the real holding time necessary for the inhibition rupture t_c is plotted in logarithmic scale against the reciprocal of experimental holding temperature $T_{hold,exp}$ for the different Ti IF steels studied (Figure 6). Straight lines are obtained in all cases. This indicates that the time necessary for the inhibition layer breakdown does indeed vary with temperature according to an Arrhenius-type law. The values of E_a and $Q_c/\left(D_0\left|\nabla c_{Zn}^{i.l.}\right|\right)$ extracted from Figure 6 for the different steels are presented in table 3.

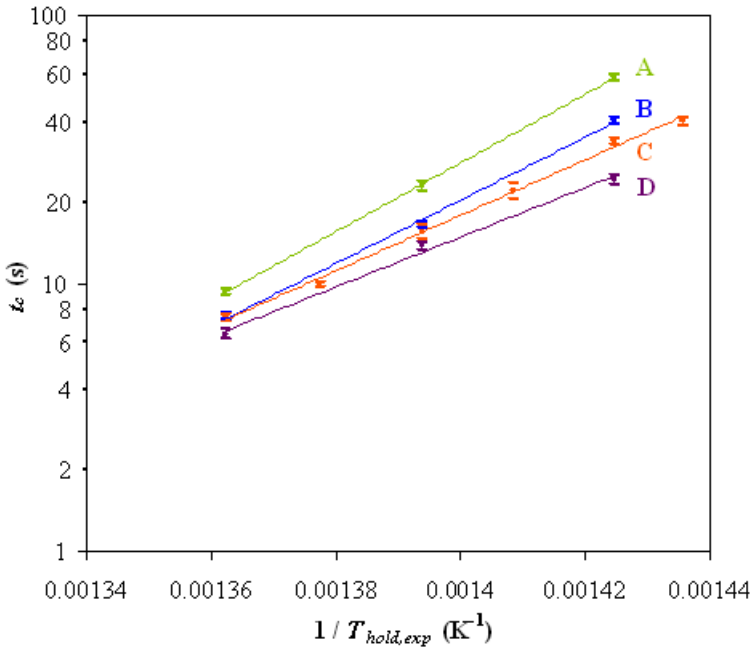

Figure 6 Real holding time needed for the inhibition layer breakdown (logarithmic scale) against the reciprocal of the experimental holding temperature.

Table 3 Values of $x_{Ti_{excess}}$, E_a and $Q_c/\left(D_0\left|\nabla c_{Zn}^{i.l.}\right|\right)$ for the Ti IF steels studied.

Steel	$x_{Ti_{excess}}$	E_a (J/mol)	$Q_c/\left(D_0\left\|\nabla c_{Zn}^{i.l.}\right\|\right)$ (s)
A	0.7	245500	3.2×10^{-17}
B	1.8	225500	6.6×10^{-16}
C	2.7	198300	5.7×10^{-14}
D	4.2	177600	1.5×10^{-12}

In the model proposed here (equation 2), the diffusion through the inhibition layer only is considered. Therefore, the values of E_a and D_0 obtained should not vary with the steel grade. The differences in reactivity should only be linked to different values of Q_c, the quantity of Zn needed to cause the inhibition layer breakdown. However, as it can be seen in figure 6, the slopes of the straight lines are different for each steel: the value of E_a varies from one steel to another and cannot finally be considered as the activation energy of Zn diffusion through the inhibition layer. This energy must so be interpreted as the activation energy of Zn diffusion in the grain boundaries, the actual rate limiting step, which varies with $x_{Ti_{excess}}$.

The activation energy E_a decreases while the parameter $Q_c/\left(D_0\left|\nabla c_{Zn}^{i.l.}\right|\right)$ increases when $x_{Ti_{excess}}$ increases (table 3). When the value of $x_{Ti_{excess}}$ is higher, the grain boundaries are cleaner. In this case, Zn diffusion in the grain boundaries is faster and the corresponding E_a is lower. However, a higher amount of Zn flux is needed to trigger the outburst reaction, because it requires a certain amount of Zn to be accumulated in a critical volume to stabilize the first nuclei of Γ phase.

No experiment at higher temperature has been performed in this work but figure 6 suggests that an inversion of the steel reactivity should be observed when the temperature increases enough. Accumulating the critical amount of Zn in the required volume for the nucleation of the first Γ nuclei can indeed become less rapid in the steel with too clean grain boundaries.

CONCLUSIONS

- The inhibition layer breakdown by outburst formation occurs through Zn diffusion in the steel grain boundaries and nucleation of a Fe-Zn phase at these locations. A sequence of reaction mechanisms accounting for this phenomenon has been proposed and explained by means of the concept of diffusion paths in the Al-Fe-Zn ternary phase diagram at the galvannealing temperature. The diffusion of Zn towards the steel enriches the steel / inhibition layer interface in this element. As a result of this enrichment, the disappearance of the $Fe_2Al_5Zn_x$ layer occurs first, stabilizing a steel / δ interface. Further enrichment of the steel grain boundaries in Zn leads to the nucleation of the Γ phase at these locations, which breaks the inhibition layer off locally.

- Trying to describe the inhibition layer breakdown kinetics by a simplified Zn diffusion model through the inhibiting layer only does not hold. A diffusion model has to take into account Zn diffusion into the steel grain boundaries.

- The effect of the steel chemical composition on the inhibition layer breakdown kinetics has been investigated. The parameter $x_{Ti_{excess}}$ proposed in this study seems to successfully describe the cleanliness of the steel grain boundaries and, consequently, the reactivity of the steel with respect to the inhibition layer breakdown. The experimental results obtained at holding temperatures from 425 to 460 °C have shown that high values of $x_{Ti_{excess}}$, corresponding to the clean grain boundaries, accelerate the inhibition layer breakdown. This behaviour is predicted to be reversed for higher temperatures, when the critical amount of Zn in the grain boundaries required for Γ nucleation should be reached first for steels with lower $x_{Ti_{excess}}$.

REFERENCES

1) M.-L. Giorgi, J.-B. Guillot and R. Nicolle: J. Mater. Sci., 40 (2005), 2263.
2) D. Zapico Álvarez, F. Bertrand, J.-M. Mataigne and M.-L. Giorgi: Proc. of the 9th Int. Conf. on Zinc and Zinc Alloy Coated Steel Sheet, Beijing, (2013), 743.
3) E. T. McDevitt and M. Meshii: Zinc-Based Steel Coating Systems: Production and Performance, Proc. of the Int. Symp., ed. by F. E. Goodwin, TMS, Warrendale, PA, USA, (1998), 127.
4) H. Nitto, T. Yamazaki, N. Morita, K. Yabe and S. Bandoo: Tetsu–to–Hagane, 70 (1984), 1719.
5) A. Nishimoto, J. Inagaki and K. Nakaoka: Trans. ISIJ, 26 (1986), 807.
6) M. Úředníček and J. S. Kirkaldy: Z. Met.kd., 64 (1973), 899.
7) H. Yamaguchi and Y. Hisamatsu: Trans. ISIJ, 19 (1979), 649.
8) Y. Hisamatsu: Proc. of the 1st Int. Conf. on Zinc and Zinc Alloy Coated Steel Sheet, Tokyo, (1989), 3.
9) Y. Leprêtre: Étude des mécanismes réactionnels de la galvanisation, PhD Thesis, Université Paris XI Orsay, (1996).
10) Y. Leprêtre, J.-M. Mataigne, M. Guttmann and J. Philibert: Zinc-Based Steel Coating Systems: Production and Performance, Proc. of the Int. Symp., ed. by F. E. Goodwin, TMS, Warrendale, PA, USA, (1998), 95.
11) C. E. Jordan and A. R. Marder: Metall. Mater. Trans. A, 28A (1997), 2683.
12) C. E. Jordan and A. R. Marder: Zinc-Based Steel Coating Systems: Production and Performance, Proc. of the Int. Symp., ed. by F. E. Goodwin, TMS, Warrendale, PA, USA, (1998), 115.
13) M. Guttmann: Mat. Sci. Forum, 155–156 (1994), 527.
14) J.-M. Mataigne: Rev. Métall., 106 (2009), 27.
15) M. Guttmann, Y. Leprêtre, A. Aubry, M. J. Roch, T. Moreau, P. Drillet, J.-M. Mataigne and H. Baudin: Proc. of the 3rd Int. Conf. on Zinc and Zinc Alloy Coated Steel Sheet, Chicago, (1995), 295.
16) S. Dionne, G. Botton, M. Charest and F. Goodwin: Proc. of Int. Symp. on Materials in the Automotive Industry, Toronto, (2001), 351.
17) M. Saito, Y. Uchida, T. Kittaka, Y. Hirose and Y. Hisamatsu: Tetsu-to-Hagane, 77 (1991), 947.
18) J.-S. Kim and J. H. Chung: Zinc-Based Steel Coating Systems: Production and Performance, Proc. of the Int. Symp., ed. by F. E. Goodwin, TMS, Warrendale, PA, USA, (1998), 157.
19) T. Toki, K. Oshima, T. Nakamori, Y. Saito, T. Tsuda and Y. Hobo: The Physical Metallurgy of Zinc Coated Steel, ed. by A. R. Marder, TMS, Warrendale, PA, USA, (1994), 169.
20) M. Abe and S. Kanbara: Tetsu-to-Hagane, 69 (1983), S1061.